JOURNAL OF Applied Polymer SCIENCE

Intercalated Clay Structures and Amorphous Behavior of Solution Cast and Melt Pressed Poly(ethylene oxide)–Clay Nanocomposites

Shobhna Choudhary, Ram Jeewan Sengwa
Dielectric Research Laboratory, Department of Physics, J N V University, Jodhpur 342 005, India
Correspondence to: S. Choudhary (E-mail: shobhnachoudhary@rediffmail.com)

ABSTRACT: The polymer nanocomposite (PNC) films consisted of poly(ethylene oxide) (PEO) and sodium cations montmorillonite (MMT) clay were prepared by aqueous solution casting and direct melt press compounding techniques, whereas the films of PEO with trimethyl octadecyl ammonium cations organo-modified montmorillonite (OMMT) clay were formed by melt pressed technique. The clay concentrations in the nanocomposites used are 1, 2, 3, 5, 10, and 20 wt % of the PEO weight. The X-ray diffraction patterns of these nanocomposites were measured in the angular range (2θ) of 3.8–30°. The values of basal spacing d_{001} of MMT/OMMT, clay gallery width W_{cg}, d-spacings of PEO crystal reflections d_{120} and d_{112}, and their corresponding crystallite size L, and the peaks intensity I (counts) were determined for these nanocomposites. Results reveal that the nanocomposites have intercalated clay structures and the amount of intercalation increases with the increase of clay concentration. As compared to melt pressed PEO–MMT nanocomposites, the amount of clay intercalation is higher in aqueous solution cast nanocomposites. At 20 wt % MMT dispersion in PEO matrix, the solution cast PEO–MMT nanocomposite almost changes into amorphous phase. The melt press compounded PEO–OMMT films show more intercalation as compared to the PEO–MMT nanocomposites prepared by same technique. In melt pressed nanocomposites, the PEO crystalline phase significantly reduces when clay concentration exceeds 3 wt %, which is evidenced by the decrease in relative intensity of PEO principal crystalline peaks. The effect of interactions between the functional group (ethylene oxide) of PEO and layered sheets of clay on both the main crystalline peaks of PEO was separately analyzed using their XRD parameters in relation to structural conformations of these nanocomposites. © 2013 Wiley Periodicals, Inc. J. Appl. Polym. Sci. **2014**, *131*, 39898.

KEYWORDS: clay; composites; crystallization; X-ray; hydrophilic polymers

Received 17 April 2013; accepted 25 August 2013
DOI: 10.1002/app.39898

INTRODUCTION

In the last two decades, polymer nanocomposites (PNCs) have emerged a new class of materials due to not only scientific interest but also the remarkable improvement in the performance properties of host polymer matrix dispersed with extremely small amount of clay as inorganic nanofiller.[1–3] Among the polymer nanocomposites, the poly(ethylene oxide) (PEO) dispersed with Na^+–montmorillonite (abbreviated as MMT or Na^+–MMT clay) layered has attracted special interest due to its many technical applications in the area of solid polymer electrolytes, pharmaceutical drugs, purification of biological materials, adhesives, packaging and surface coating films, friction reduction, thickening of water-based paints, etc.[3–22] The MMT has 2:1 charged phyllosilicate platelets of 1 nm thickness and these are stacked by weak dipolar or van der Waals forces which lead to the intercalation of polar molecules causing the crystal lattice to expand in the c-direction. Both PEO and MMT have hydrophilic behavior due to which the PEO partially adsorbs on the MMT platelets surfaces besides the intercalation in MMT basal interlayer galleries.[6–10,13]

The earlier studies on PEO–MMT nanocomposites by different spectroscopic, morphological, and mechanical techniques established that the interactions between MMT and PEO at molecular level substantially improve mechanical, thermal, optical, chemical, and gas permeable properties of the nanocomposite as compared to the pure PEO matrix.[3–16] The control and optimization of these useful properties are expected to enable the development of PNC materials with predefined superior properties for their industrial applications. The degree of exfoliated/intercalated MMT structures in polymer matrix also has great importance in tailoring the dielectric properties along with physical properties of the PNCs, which established their suitability as novel dielectric/insulating materials in integrated electronics, membrane technology and in the solid state electrolytes.[17–42]

The MMT structures in polymer matrix are significantly governed by their preparation techniques. Mostly solution casting

and melt compounding techniques are used for the synthesis of PNC materials. Due to low melting temperature and good film forming ability of high molecular weight PEO, it is a model system often used to understand the fundamental behavior of polymer interactions and adsorption with inorganic nanofillers. Survey of literature reveals that there is scarcity of comparative structural parameters of PEO–MMT nanocomposites prepared by solution cast and melt pressed techniques. Further, the comparative structural study of PEO based sodium cations MMT, and the trimethyl octadecyl ammonium cations surface modified MMT, i.e., also known as organo-modified MMT (OMMT) nanocomposites prepared by melt pressed technique were not explored, so far.

In this article, an attempt is made to confirm the comparative structural behavior and amorphicity of aqueous solution cast PEO–MMT and melt press compounded PEO–MMT/OMMT nanocomposite films by X-ray diffraction (XRD) measurements. This study has been performed with the aim to explore the effect of blending processes on intercalated structures of MMT dispersed in PEO matrix. Further, the PNCs were prepared by melt pressed technique using trimethyl octadecyl ammonium cations MMT (OMMT) dispersed in PEO matrix in order to confirm the effect of the long chain length oniums on the intercalated structures as compared to the simple Na^+–MMT intercalated structures formed in melt PEO solvent during their melt processing.

EXPERIMENTAL

Materials

The PEO of molecular weight 600,000 g/mol, polymer grade hydrophilic Na^+–montmorillonite (MMT) (Nanoclay, Nanomer® PGV), and organically treated montmorillonite (OMMT) clay (Nanocor® 1.28 E) were purchased from Sigma-Aldrich. The MMT is white in color, and has 145 meq/100 g cation exchange capacity, 150–200 aspect ratio, 2.6 g/cc specific gravity, and 9–10 pH value on 5% dispersion. The OMMT powder is off white, and it has onium surface modification of 25–30 wt % trimethyl stearyl ammonium cations as reported by the manufacturer. This was achieved by octadecyl trimethyl ammonium chloride through cations exchanged process, thus allowing it to interface with different polymer matrices.

Preparation of PEO–x wt % MMT/OMMT Nanocomposite Films

The PEO−x wt % MMT nanocomposite films of varying MMT concentration, x up to 20 wt %, were prepared by aqueous solution-casting and direct melt press compounding techniques, whereas PEO–x wt % OMMT films were prepared by direct melt press compounding technique. Initially for the preparation of solution cast PNCs films, the required amounts of MMT (for $x = 1$, 2, 3, 5, 10, and 20 wt % of the PEO weight) were added in double distilled deionized water in air tight caped glass bottles. The MMT hydrocolloids of each sample were achieved by vigorous stirring using Teflon coated magnetic stir bar on a magnetic stir plate for two days at room temperature. After that the respective amounts of PEO (corresponding to the MMT concentrations) were added

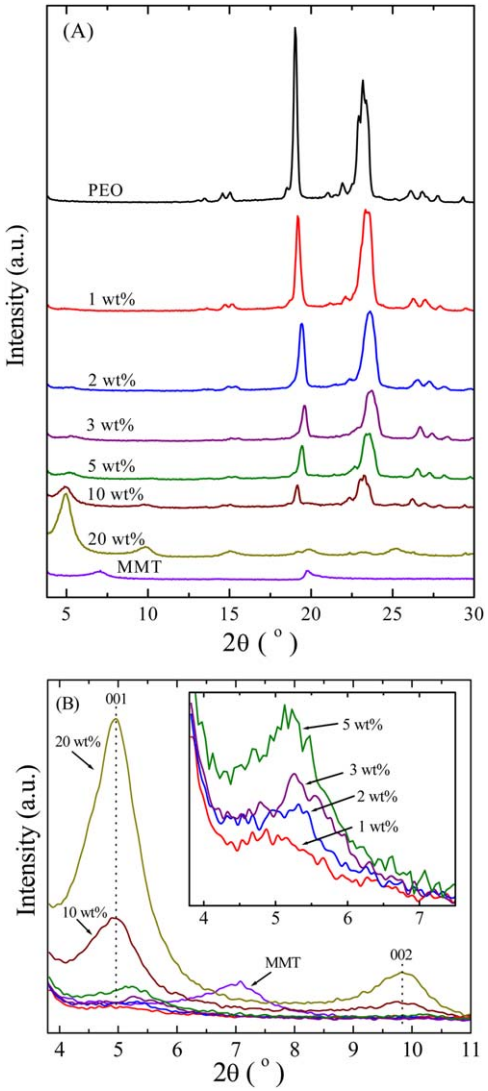

Figure 1. (A) XRD of MMT powder and aqueous solution cast prepared pure PEO and PEO–x wt % MMT nanocomposites and (B) magnification of the small 2θ region on same intensity scale. [Color figure can be viewed in the online issue, which is available at wileyonlinelibrary.com.]

to the MMT hydrocolloids and left the solutions for 2 days to dissolve the added PEO, properly. These colloidal solutions were vigorously magnetic stirred for 2 h to promote the PEO intercalation in the MMT galleries. The PEO−x wt % MMT nanocomposite films were achieved by casting the prepared hydrocolloidal viscous solutions onto polypropylene petri dishes of 60 mm diameter and drying at room temperature for 1 week. These films were further dried under vacuum at 40°C for 24 h to remove the water traces, if any. The melt press compounded PEO–x wt % MMT and PEO–x wt % OMMT nanocomposite films were prepared by hot press polymer film making unit. For this purpose, initially the required amounts of MMT/OMMT of varying concentrations were mixed in the respective amounts of PEO. Each homogenous mixture prepared by agate and mortar was melted in stainless steel die with suitable spacer at 80°C (above the

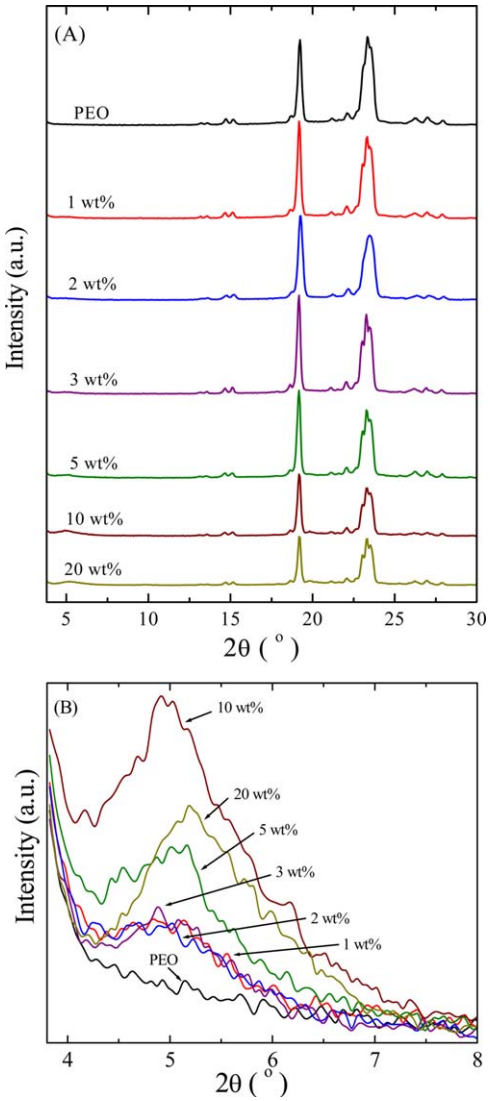

Figure 2. (A) XRD of melt pressed prepared pure PEO and PEO–*x* wt % MMT nanocomposite films and (B) magnification of 2θ on same intensity scale. [Color figure can be viewed in the online issue, which is available at wileyonlinelibrary.com.]

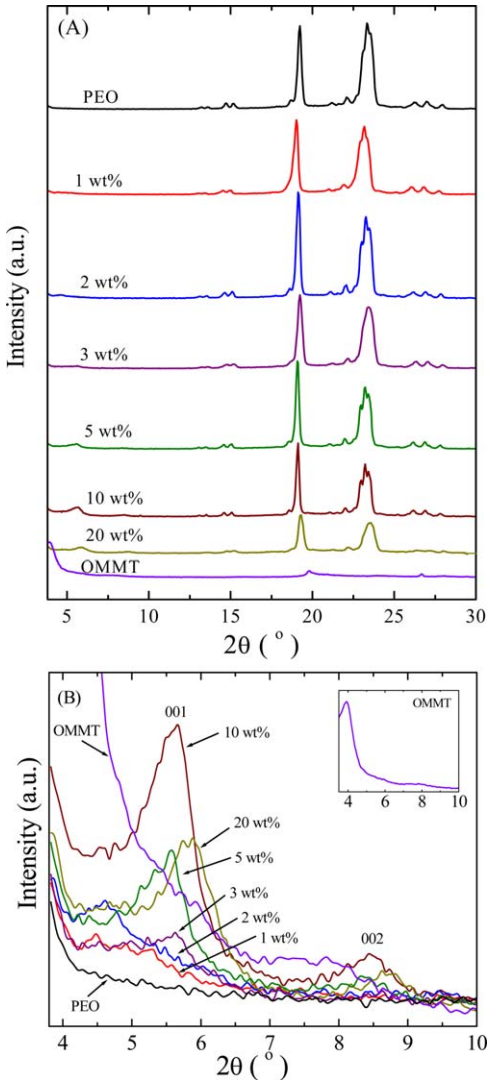

Figure 3. (A) XRD of OMMT powder and melt pressed prepared pure PEO and PEO–*x* wt % OMMT nanocomposite films and (B) magnification of the small 2θ region on same intensity scale. [Color figure can be viewed in the online issue, which is available at wileyonlinelibrary.com.]

melting temperature of PEO, i.e., 65°C) and after that the melt composition was pressed under two tons of pressure per unit area. Finally, the free standing melt press compounded nanocomposite films were achieved by slow cooling of the melt pressed materials up to room temperature.

XRD Measurements

The XRD patterns of MMT and OMMT powders, and PEO–*x* wt % MMT and PEO–*x* wt % OMMT nanocomposite films were recorded using PANalytical X′pert Pro MPD diffractometer of Cu *K*α radiation (1.5406 Å) operated at 45 kV and 40 mA with a scanned step size of 0.05° and time for each step 1 s. The powder samples of MMT and OMMT were tightly filled in the sample holder whereas the PNC films were placed on the top of sample holder for their XRD measurements in the 2θ range from 3.8° to 30°, at room temperature.

RESULTS AND DISCUSSION

The XRD patterns of MMT powder, solution cast pure PEO film and PEO–*x* wt % MMT nanocomposite films are shown in Figure 1(A,B). Figure 2(A,B) shows the XRD patterns of melt pressed pure PEO and PEO–*x* wt % MMT films, whereas Figure 3(A,B) depicts the XRD patterns of OMMT powder and melt pressed PEO–*x* wt % OMMT nanocomposite films. The characteristics features of the XRD patterns (Figures 1–3) are (i) the MMT peak at $2\theta = 7.03°$ and OMMT peak at $2\theta = 3.91°$ are referred to the d_{001} basal spacing of the MMT and OMMT nanoplatelets while the other peak around 19.79° observed for both the clays can be related to the impurities (mostly quartz and feldspar) presented in MMT/OMMT.[32,38] In addition to these peaks, OMMT also shows the peak corresponding to d_{002} basal spacing at $2\theta = 7.83°$, (ii) the main crystalline peaks

Table I. Bragg's Angle 2θ, Basal Spacing d, Full Width at Half Maximum FWHM, Crystallite Size L, Intensity (counts) I, and Clay Gallery Width Wcg of Aqueous Solution Cast Prepared PEO–x wt % MMT Nanocomposite Films

Parameters of 001 reflection peak of MMT						
x wt % MMT	2θ (°)	d_{001} (nm)	W_{cg} (nm)	I_{001} (counts)		
MMT	7.03	1.257	0.297	520		
1	4.87	1.815	0.855	64		
2	5.37	1.646	0.686	135		
3	5.29	1.670	0.710	211		
5	5.20	1.698	0.738	303		
10	4.97	1.775	0.815	1119		
20	4.96	1.779	0.819	4149		
Parameters of 120 reflection peak of PEO						
x wt % MMT	2θ (°)	d_{120} (nm)	$FWHM_{120}$ (rad)	L_{120} (nm)	I_{120} (counts)	RI_{120} (%)
PEO	19.03	0.466	0.0044	33.52	15296	100.0
1	19.20	0.462	0.0056	26.30	8058	52.7
2	19.47	0.456	0.0060	24.47	5749	37.6
3	19.62	0.452	0.0051	28.54	2926	19.1
5	19.48	0.455	0.0051	28.54	2770	18.1
10	19.16	0.463	0.0043	34.21	1885	12.3
20	19.93	0.445	0.0069	21.38	550	3.6
Parameters of 112,032 reflection peak of PEO						
x wt % MMT	2θ (°)	d_{112} (nm)	$FWHM_{112}$ (rad)	L_{112} (nm)	I_{112} (counts)	RI_{112} (%)
PEO	23.22	0.383	0.0132	11.18	9515	100.0
1	23.44	0.379	0.0131	11.27	8594	90.3
2	23.59	0.377	0.0144	10.29	6965	73.2
3	23.65	0.376	0.0148	9.97	4406	46.3
5	23.48	0.379	0.0145	10.22	4048	42.5
10	23.18	0.383	0.0145	10.17	2659	27.9
20	23.05	0.386	0.0069	21.49	283	2.9

appearing at 19.03° and 23.22° for solution cast prepared PEO film, and at 19.22° and 23.41° for melt pressed PEO film can be attributed to crystal reflection planes 120 and concerted 112,032 of the PEO crystalline phases[13,31] which are supported by low intensity peaks on both sides, and (iii) the peak appearing corresponding to basal spacing d_{001} of MMT and its shift toward lower angle side for PNCs, and also the decrease in intensity of PEO main peaks confirm the formation of MMT/OMMT intercalated structures and strong complexations of PEO with MMT/OMMT in the nanocomposite films.[5,6,8,11]

The peak position (2θ) and intensity I (counts) values of 001 reflection planes of MMT/OMMT, and 120 and 112,032 crystalline planes of pure PEO and PNCs were determined using X'pert pro® software. The values of d-spacing corresponding to these crystalline peaks were determined by the Bragg's relation $\lambda = 2d \sin\theta$, where λ is the wavelength of X-ray radiation ($\lambda = 1.5406$ Å), d is the spacing between diffractional lattice planes, and θ is the measured diffraction angle of the respective peaks. The values of 2θ, d-spacing and I for different nanocomposites are recorded in Tables I–III. The observed 2θ values of PEO main crystalline peaks and the 001 peak of MMT were found in good agreement with the literature values.[10,13] The values of mean crystallite size L in the direction perpendicular to (hkl) plane of the nanocomposites were evaluated by Scherrer's equation $L = \lambda k/\beta\cos\theta$, where $k = 0.94$ is a constant and β is full width at half maximum (FWHM) (the broadening of peak at half-height expressed in radians of 2θ, i.e., width measured in 2θ degrees and then multiplied by $\pi/180$). The relative intensity RI is determined by $RI\ (\%) = I_{PNC}/I_{PEO} \times 100$, where I_{PNC} and I_{PEO} are the respective intensity counts of PNC and pure PEO (I_{PEO} of SC prepared pure PEO film for solution cast nanocomposites and I_{PEO} of MP prepared pure PEO film for melt press compounded are used). The evaluated values of L, FWHM and RI of the nanocomposites are also recorded in Tables I–III.

In order to examine the effect of MMT/OMMT concentration on their intercalated structures in PEO matrix, the magnified view of small angle XRD patterns of PEO–x wt % MMT/OMMT nanocomposites are depicted in Figures 1(B)–3(B). These XRD spectra show that the 001 peaks of PEO–x wt %

Table II. Bragg's Angle 2θ, Basal Spacing d, Full Width at Half Maximum FWHM, Crystallite Size L, Intensity (counts) I, and Clay Gallery Width Wcg of Direct Melt Pressed Prepared PEO–x wt % MMT Nanocomposite Films

Parameters of 001 reflection peak of MMT						
x wt % MMT	2θ (°)	d_{001} (nm)	W_{cg} (nm)	I_{001} (counts)		
MMT	7.028	1.257	0.297	520		
1	5.13	1.721	0.761	68		
2	5.01	1.762	0.802	84		
3	4.89	1.806	0.846	143		
5	5.16	1.711	0.751	202		
10	5.03	1.755	0.795	405		
20	5.23	1.688	0.728	347		
Parameters of 120 reflection peak of PEO						
x wt % MMT	2θ (°)	d_{120} (nm)	$FWHM_{120}$ (rad)	L_{120} (nm)	I_{120} (counts)	RI_{120} (%)
PEO	19.22	0.461	0.0047	31.28	12964	100.0
1	19.18	0.462	0.0044	33.53	14672	113.2
2	19.26	0.460	0.0056	26.47	12948	99.9
3	19.16	0.463	0.0040	36.27	15020	115.9
5	19.17	0.463	0.0043	34.49	13321	102.8
10	19.18	0.462	0.0043	34.49	9476	73.1
20	19.19	0.462	0.0039	37.40	7078	54.6
Parameters of 112,032 reflection peak of PEO						
x wt % MMT	2θ (°)	d_{112} (nm)	$FWHM_{112}$ (rad)	L_{112} (nm)	I_{112} (counts)	RI_{112} (%)
PEO	23.41	0.380	0.0131	11.27	12569	100.0
1	23.40	0.380	0.0132	11.22	11471	91.3
2	23.48	0.379	0.0131	11.25	9649	76.8
3	23.28	0.382	0.0128	11.56	11800	93.9
5	23.39	0.380	0.0132	11.19	9294	73.9
10	23.40	0.380	0.0132	11.19	6753	53.7
20	23.32	0.381	0.0126	11.73	6779	53.9

MMT nanocomposites are at lower angle side as compared to the MMT powder (Tables I–III) which reveals the formation of MMT intercalated structures. In this intercalation process, the PEO chains occupied the galleries of MMT layers. The 001 peaks of PEO–x wt % OMMT were found towards higher angle side as compared to the OMMT peak, which is due to intercalation of PEO ordered structures in OMMT galleries those were occupied earlier by trimethyl stearyl ammonium cations. In the case of OMMT based nanocomposite, it is expected that there is large possibility of PEO ordered structures formation in the galleries with the displacement of bulky cations when the melt composition of the materials were pressed under 2 tons of pressure during their preparation process. The intercalation occurs mainly due to favorable interactions between the hydroxyl groups of MMT nanoplatelets surfaces and the oxygen atoms of PEO chain. The roughly comparable distances (~2.8 Å) between adjacent oxygen atoms in linear PEO chain and the inter hydroxyl groups of MMT make the PEO and MMT interactions particularly more favourable.[5] The exfoliated MMT no longer displays the 001 reflection peak, but the extend of exfoliation is, however, believed to be moderate because the 001 peaks of the PEO–x wt % MMT nanocomposites are very sharp, even sharper than for the pure MMT powder.

Figure 4 shows that the intensity values of 001 reflection peak I_{001} have an increase with the increase of MMT/OMMT concentration in these PNC materials. As compared to melt pressed nanocomposites, significantly high I_{001} values of solution cast nanocomposites at the same concentration of MMT reveal that a large amount of PEO intercalation occurs when PEO–x wt % MMT nanocomposites are synthesized by solution casting technique. It seems that swelled MMT becomes more active in aqueous solutions to intercalate the PEO in their galleries. Further, from Figure 4, it is observed that the 001 peak intensity of OMMT based melt compounded nanocomposites are comparatively higher than that of the MMT based melt pressed PNCs. These comparative results reveal that the OMMT promotes more amount of PEO intercalation as compared to unmodified MMT, which is obviously because of the larger gallery size ($d_{001} = 2.258$ nm) of the OMMT. Figure 4 also shows the variation of d_{001} values of the PNCs with x wt % MMT/OMMT. The PEO–x

Table III. Bragg's Angle 2θ, Basal Spacing d, Full Width at Half Maximum FWHM, Crystallite Size L, Intensity (counts) I, and Clay Gallery Width Wcg of Direct Melt Pressed Prepared PEO–x wt % OMMT Nanocomposite Films

Parameters of 001 reflection peak of OMMT						
x wt % OMMT	2θ (°)	d_{001} (nm)	W_{cg} (nm)	I_{001} (counts)		
OMMT	3.91	2.258	1.298	103		
1	5.28	1.672	0.712	39		
2	4.63	1.907	0.947	154		
3	5.64	1.566	0.606	183		
5	5.57	1.585	0.625	567		
10	5.62	1.571	0.611	992		
20	5.86	1.507	0.547	637		
Parameters of 120 reflection peak of PEO						
x wt % OMMT	2θ (°)	d_{120} (nm)	$FWHM_{120}$ (rad)	L_{120} (nm)	I_{120} (counts)	RI_{120} (%)
PEO	19.22	0.461	0.0047	31.28	12964	100.0
1	19.02	0.466	0.0055	26.62	11588	89.4
2	19.14	0.463	0.0047	31.51	16641	128.4
3	19.24	0.461	0.0059	24.90	11379	87.8
5	19.09	0.465	0.0040	36.58	13829	106.7
10	19.11	0.464	0.0038	39.14	11124	85.87
20	19.29	0.460	0.0062	23.84	6065	46.8
Parameters of 112,032 reflection peak of PEO						
x wt % OMMT	2θ (°)	d_{112} (nm)	$FWHM_{112}$ (rad)	L_{112} (nm)	I_{112} (counts)	RI_{112} (%)
PEO	23.41	0.380	0.0131	11.27	12569	100.0
1	23.19	0.383	0.0131	11.29	9776	77.8
2	23.35	0.381	0.0134	11.06	11545	91.9
3	23.44	0.379	0.0131	11.28	9281	73.8
5	23.27	0.382	0.0132	11.19	8603	68.4
10	23.23	0.383	0.0128	11.54	7809	62.1
20	23.51	0.378	0.0131	11.32	4494	35.8

wt % MMT nanocomposites have significant increase of d_{001} values when a small amount of MMT (1 wt %) is dispersed in the PEO matrix, which have little variations with further increase of MMT concentration. In the case of PEO–x wt % OMMT, the d_{001} value has a large drop when 1 wt % OMMT is added and it approaches close to that of the MMT based nanocomposites, which also have less variations with further increase of OMMT concentration in the PNC materials.

The values of change in MMT clay gallery W_{cg} are estimated from the relation $W_{cg} = d_{001} - W_{cl}$, where W_{cl} is MMT clay layer width in c-axis, which is 9.6 Å (0.96 nm) for the pure clay.[31] The evaluated values of W_{cg} of the different nanocomposites are given in Tables I–III. Table I shows that the d_{001} spacing for MMT powder is 1.26 nm (12.6 Å), and corresponding W_{cg} value is 0.297 nm, which is mostly occupied by hydrated cations of the natural clay and these are exchangeable.[31] The loading of 1 wt % MMT in PEO matrix changes the d_{001} spacing up to 1.81 nm, which results the $W_{cg} = 0.855$ nm when the PEO–MMT nanocomposite is prepared by solution casting technique. This W_{cg} value represents that the bilayer structure of PEO or helical structure arranged in flattened arrangements can be accommodated because the *trans*-conformation of PEO chain has an expansion of about 0.4 nm.[5,19] The intercalated 0.80 nm wide *trans*-gauche-*trans* double layers structures of PEO and poly(ethylene glycol) (PEG) are the most stable arrangement from steric consideration.[6,19,43–45] Further increase of MMT concentration in the solution cast nanocomposite films, the observed W_{cg} values range from 0.686–0.855 nm (Table I), which also confirms the existence of flattened bilayers arrangement of PEO structures in the MMT galleries. The W_{cg} values of melt pressed PEO–x wt % MMT and the PEO–x wt % OMMT nanocomposites (Tables II and III, respectively) also infer the well-ordered bilayer morphology of PEO intercalated structures in the clay galleries and this morphology remains almost same with increase of MMT/OMMT concentration. Further, at 10 and 20 wt % MMT concentration, the 002 reflection peak of clay is also immersed around $2\theta \approx 10°$ [Figure 1(B)], which suggests the increase of intercalated MMT phase at these concentrations in the aqueous solution cast nanocomposites.

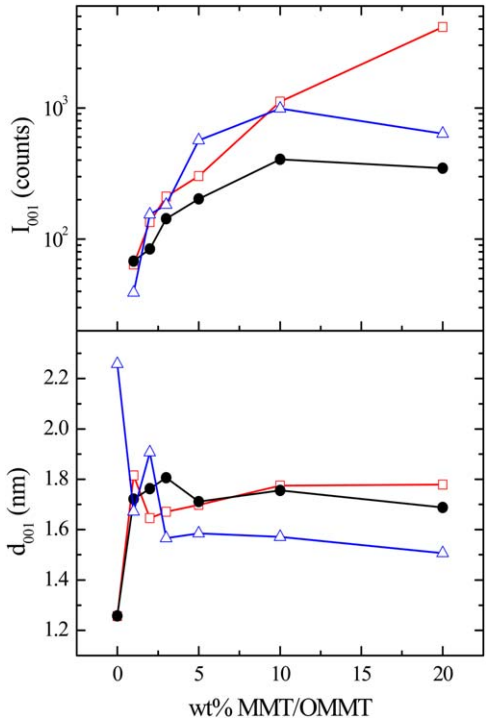

Figure 4. Variation of I_{001} and d_{001} values with clay concentration of the nanocomposites; (□) solution cast PEO–*x* wt % MMT, (●) melt pressed PEO–*x* wt % MMT, and (Δ) melt pressed PEO–*x* wt % OMMT. [Color figure can be viewed in the online issue, which is available at wileyonlinelibrary.com.]

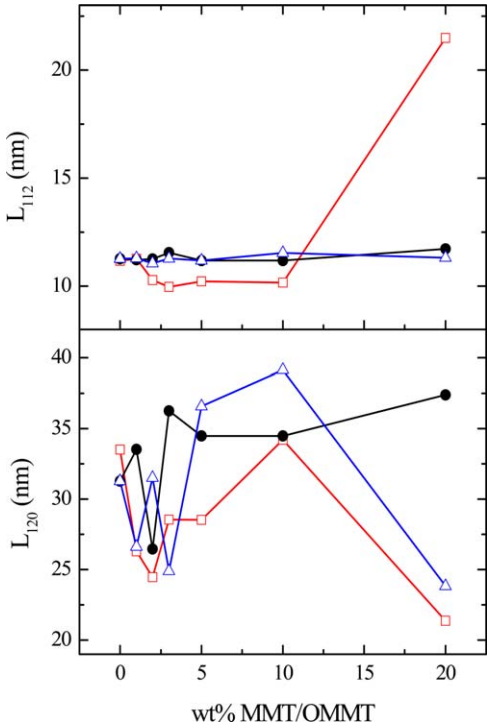

Figure 5. Variation of L_{120} and L_{112} values with clay concentration of the nanocomposites; (□) solution cast PEO–*x* wt % MMT, (●) melt pressed PEO–*x* wt % MMT, and (Δ) melt pressed PEO–*x* wt % OMMT. [Color figure can be viewed in the online issue, which is available at wileyonlinelibrary.com.]

The PEO and MMT peaks of these PNC films in the XRD patterns have independent entities (Figures 1–3), which reveal the multiphase characteristics comprising amorphous and crystalline components. The values of PEO main peaks (120 and 112,032) parameters, i.e., peak position, basal spacing, crystallite size, peak intensity, and peaks relative intensity of the nanocomposites are given in Tables I–III, which are interpreted in relation to confirm the effect of clay loading on each crystalline phase of PEO in the PEO–*x* wt % MMT/OMMT nanocomposites prepared by different techniques. Tables I–III show that there is a little change in the values of 2θ and *d*-spacing corresponding to 120 and 112,032 crystalline peaks of PEO with the increase of clay concentration in the nanocomposites. Further, it seems that these values are less influenced by the method of preparation and also the type of clay used in the nanocomposites. But the values of crystallite size *L*, which is a measure of the spherulites of the PEO matrix for 120 and 112,032 reflections of PEO changes with clay concentration. Figure 5 shows that the values of L_{120} corresponding to 120 peak reflections of PEO vary anomalously with the increase of clay concentration and also with their preparation techniques and the type of clay used in the nanocomposites. But it is found that the change in L_{112} values of 112,032 peak of melt pressed nanocomposites is less influenced by the type of clay and its concentration for the nanocomposites prepared by melt pressed technique, whereas L_{112} value of solution cast PNC film has large increase at 20 wt % MMT.

Figure 6 shows the variation of relative intensity *RI* of PEO main crystalline peaks with clay concentration of the PEO–*x* wt % MMT/OMMT nanocomposites. It is observed that both the RI_{120} and RI_{112} values have large decrease with increase of MMT concentration for aqueous solution cast nanocomposites, which confirms the increase in amount of amorphous phase of the nanocomposites. Here first we consider the variation of RI_{120} values of the nanocomposites with clay concentration. It is observed that at 1 wt % MMT loading, the peak intensity of aqueous solution cast PEO–MMT nanocomposite drops to 52.7%, which is nearly half of the intensity of aqueous solution cast pristine PEO film (Figure 6). This reveals that there are disruptions of PEO spherulites arrangement by large amount due to the formation of strong interactions between PEO and exfoliated MMT nanoplatelets, which increase their overall amorphous phase. At 20 wt % MMT loading in PEO matrix, the RI_{120} drops to almost zero, i.e., only 3.6%, which confirms the large damage of the PEO spherulites corresponding to the 120 peak of the aqueous solution cast PEO–20 wt % MMT nanocomposite. This fact is also supported by a large enhancement of d_{001} peak intensity for the nanocomposite at this MMT concentration [Figure 1(B)]. In polymer nanocomposites, it has been established that the enhancement of the amount of polymer intercalation in MMT galleries results the decrease of host polymer crystallinity.[13,16,34,40] The RI_{120} values of melt pressed synthesized both the PEO–*x* wt % MMT and PEO–*x* wt % OMMT nanocomposites have anomalous variation up to 5 wt

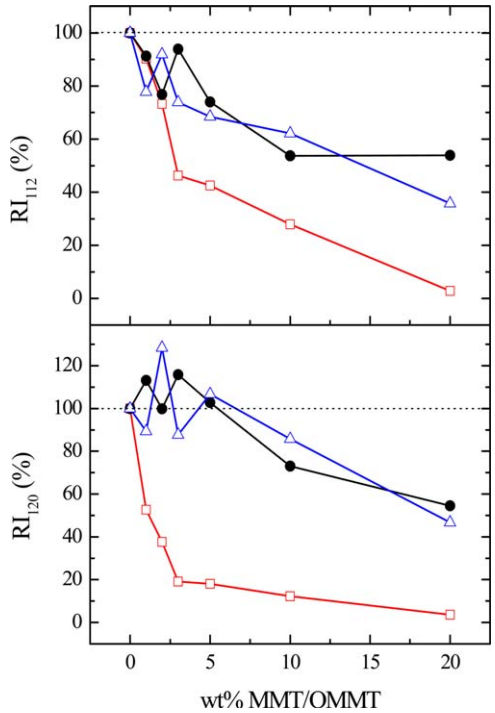

Figure 6. Variation of RI_{120} and RI_{112} values with clay concentration of the nanocomposites; (□) solution cast PEO–*x* wt % MMT, (●) melt pressed PEO–*x* wt % MMT, and (Δ) melt pressed PEO–*x* wt % OMMT. [Color figure can be viewed in the online issue, which is available at wileyonlinelibrary.com.]

% clay loading and their peak intensity values are close to the intensity of melt pressed pure PEO film. From these values, it seems that at low clay concentration the dispersed silicate layers act as nucleating agents for the crystallization of PEO when these PNCs are prepared by melt pressed technique, which is consistent with earlier finding on the melt mixed prepared PEO–MMT nanocomposites.[13] Further these values reveal that interaction behavior of PEO with MMT and their structures in melt compounding are entirely different as compared to that of the aqueous solution cast nanocomposites. At 10 and 20 wt % MMT/OMMT, there is significant decrease of RI_{120} values, which confirms that there is also increase of PEO amorphous phase by melt compounding but this amount is significantly less as compared to that of the solution cast nanocomposites consisted of same clay concentration. This observation is in good agreement with the earlier findings on crystalline phase of PEO in PEO–MMT nanocomposites determined by differential scanning calorimetry thermograms.[16]

The RI_{112} values of aqueous solution cast PEO–*x* wt % MMT nanocomposites also have a large decrease up to 3 wt % MMT loading, and it approaches to 2.9% when 20 wt % MMT has been dispersed in PEO matrix (Figure 6), which indicates nearly total conversion of PEO crystalline phase into an amorphous phase corresponding to 112,032 reflection planes when MMT loading exceeds the 20 wt % concentration. But, in the case of melt pressed synthesized PEO–*x* wt % MMT/OMMT nanocomposites, the RI_{112} values have anomalous decreases, and these values are about 50% of the pure PEO at 20 wt % MMT/OMMT concentration, which reveal that these materials still have a significant amount of PEO in crystalline form.

CONCLUSION

This article presents the XRD patterns and structural parameters of the aqueous solution cast PEO–*x* wt % MMT and direct melt press compounded PEO–*x* wt % MMT/OMMT nanocomposite films. The intercalation of PEO in clay galleries increases with the increase of MMT/OMMT loading, which reduces the crystalline phase of the nanocomposites. This study reveals that the loading of 1 wt % MMT converts nearly half amount of both the crystalline phases corresponding to 120 and concerted 112,032 reflection planes of PEO into amorphous, and these crystalline phases almost suppress at 20 wt % MMT loading when the PEO–*x* wt % MMT nanocomposites were prepared by aqueous solution casting technique. The effect of nanocomposite preparation techniques on the MMT intercalation and PEO crystalline phases are clearly observed. Results reveal that solution casting technique is more prominent in preparation of nanocomposites as compared to the melt press compounding, because in aqueous solutions the interactions between functional group of PEO and clay nanoplatelets become more active. Further, structural changes in melt press prepared nanocomposites are also observed with the type of clay (MMT or OMMT) dispersed in the melt PEO matrix.

ACKNOWLEDGMENTS

Authors are grateful to the DST, New Delhi for providing the experimental facilities through research project Nos. SR/S2/CMP-09/2002 and SR/S2/CMP-0072/2010, and also by the DST–FIST program. One of the authors SC is thankful to the DST, New Delhi for the award of SERB Fast Track Young Scientist research project No. SR/FTP/PS-013/2012.

REFERENCES

1. Ray, S. S.; Okamoto, M. *Prog. Polym. Sci.* **2003**, *28*, 1539.
2. Nazari, T.; Garmabi, H.; Arefazar, A. *J. Appl. Polym. Sci.* **2012**, *126*, 1637.
3. Abraham, T. N.; Siengchin, S.; Ratna, D.; Karger-Kocsis, J. *J. Appl. Polym. Sci.* **2010**, *118*, 1297.
4. Ogata, N.; Kawakage, S.; Ogihara, T. *J. Appl. Polym. Sci.* **1997**, *66*, 573.
5. Tunney, J. J.; Detellier, C. *Chem. Mater.* **1996**, *8*, 927.
6. Shen, Z.; Simon, G. P.; Cheng, Y. B. *Polymer* **2002**, *43*, 4251.
7. Shen, Z.; Simon, G. P.; Cheng, Y. B. *Eur. Polym. J.* **2003**, *39*, 1917.
8. Strawhecker, K. E.; Manias, E. *Chem. Mater.* **2003**, *15*, 844.
9. Chaiko, D. *J. Chem. Mater.* **2003**, *15*, 1105.
10. Chen, B.; Evans, J. R. G. *J. Phys. Chem.* **2004**, *108*, 14986.
11. Elmahdy, M. M.; Chrissopoulou, K.; Afratis, A.; Floudas, G.; Anastasiadis, S. H. *Macromolecules* **2006**, *39*, 5170.
12. Miwa, Y.; Drews, A. R.; Schlick, S. *Macromolecules* **2008**, *41*, 4701.

13. Homminga, D.; Goderis, B.; Dolbnya, I.; Reynaers, H.; Groeninckx, G. *Polymer* **2005**, *46*, 11359.
14. Stefanescu, E. A.; Stefanescu, C.; Dali, W. H.; Schmidt, G.; Negulescu, I. I. *Polymer* **2008**, *49*, 3785.
15. Stefanescu, E. A.; Schexnailder, P. J.; Dundigalla, A.; Negulescu, I. I.; Schmidt, G. *Polymer* **2006**, *47*, 7339.
16. Hikosaka, M. Y.; Pulcinelli, S. H.; Santilli, C. V.; Dahmouche, K.; Craievich, A. F. *J. Non-Cryst. Solids* **2006**, *352*, 3705.
17. Aranda, P.; Mosqueda, Y., Pérez-Cappe, E.; Ruiz-Hitzky, E. *J. Polym. Sci. Part B: Polym. Phys.* **2003**, *41*, 3249.
18. Tanaka, T.; Montanari, G. C.; Mülhaupt, R. *IEEE Trans. Dielect. Elect. Insul.* **2004**, *11*, 763.
19. Reinholdt, M. X.; Kirkpatrick, R. J.; Pinnavaia, T. J. *J. Phys. Chem. B* **2005**, *109*, 16296.
20. Loyens, W.; Maurer, F. H. J.; Jannasch, P. *Polymer* **2005**, *46*, 7334.
21. Chen, H. W.; Chang, F. C. *Polymer* **2001**, *42*, 9763.
22. Lombardo, P. C.; Poli, A. L.; Neumann, M. G.; Machado, D. S.; Schmitt, C. C. *J. Appl. Polym. Sci.* **2013**, *127*, 3687.
23. Mijović, J.; Lee, H.; Kenny, J.; Mays, J. *Macromolecules* **2006**, *39*, 2172.
24. Sengwa, R. J.; Choudhary, S.; Sankhla, S. *Compos. Sci. Tech.* **2010**, *70*, 1621.
25. Sengwa, R. J.; Choudhary, S. *J. Macromol. Sci. Part B: Phys.* **2011**, *50*, 1313.
26. Choudhary, S.; Sengwa, R. *J. Indian J. Pure Appl. Phys.* **2011**, *49*, 600.
27. Choudhary, S.; Sengwa, R. J. *J. Appl. Polym. Sci.* **2012**, *124*, 4847.
28. Sengwa, R. J.; Choudhary, S. *Bull. Mater. Sci.* **2012**, *35*, 19.
29. Choudhary, S.; Sengwa, R. *J. Ionics* **2011**, *17*, 811.
30. Choudhary, S.; Sengwa, R. *J. Indian J. Pure Appl. Phys.* **2011**, *49*, 204.
31. Mohapatra, S. R.; Thakur, A. K.; Choudhary, R. N. P. *J. Power Sources* **2009**, *191*, 601.
32. Sapalidis, A. A.; Katsaros, F. K.; Steriotis, Th. A.; Kanellopoulos, N. K. *J. Appl. Polym. Sci.* **2012**, *123*, 1812.
33. Aranda, P.; Ruiz-Hitzky, E. *Chem. Mater.* **1992**, *4*, 1395.
34. Aranda, P.; Ruiz-Hitzky, E. *Appl. Clay Sci.* **1999**, *15*, 119.
35. Reading, M.; Vaughan, A. S. *CEIDP IEEE Conference Publication* **2008**, pp 579–582.
36. Pandis, C.; Logakis, E.; Peoglos, V.; Pissis, P.; Omastová, M.; Mravćáková, M.; Janke, A.; Pionteck, J.; Peneva, Y.; Minkova, L. *J. Polym. Sci.: Part B: Polym. Phys.* **2009**, *47*, 407.
37. Wang, H. W.; Shieh, C. F.; Chang, K. C.; Chu, H. C. *J. Appl. Polym. Sci.* **2005**, *97*, 2175.
38. Cardoso, J.; Montiel, R.; Manero, O. *J. Appl. Polym. Sci.* **2011**, *119*, 1357.
39. Kaya, A. U.; Esmer, K.; Tekin, N.; Beyaz, S. K. *J. Appl. Polym. Sci.* **2011**, *120*, 874.
40. Chen, B.; Evans, J. R. G.; Holding, S. *J. Appl. Polym. Sci.* **2004**, *94*, 548.
41. Chen, B.; Evans, J. R. G.; Greenwell, H.C.; Boulet, P.; Coveney, P. V.; Bowden, A. A.; Whiting, A. *Chem. Soc. Rev.* **2008**, *37*, 568.
42. Zhen, W.; Lu, C.; Li, C.; Liang, M. *Appl. Clay Sci.* **2012**, *57*, 64.
43. Kuppa, V.; Manias, E. *J. Chem. Phys.* **2003**, *118*, 3421.
44. Vasilyev, G. B.; Makarova, V. V.; Rebrov, A. V., Picken, S. J.; Smirnova, N. M.; Malkin, A. Ya., Kulichikhin, V. G. *J. Appl. Polym. Sci.* **2011**, *120*, 3642.
45. Zhu, S.; Chen, J.; Li, H.; Cao, Y. *Appl. Surf. Sci.* **2013**, *264*, 500.